# Single-photon emitter based on an ensemble of lattice-trapped interacting atoms

Deshui Yu*

*School of Physics and Astronomy, The University of Nottingham, Nottingham NG7 2RD, United Kingdom*

(Received 21 April 2014; published 13 June 2014)

Precisely controlling the atom number challenges the single-photon generation based on an individual neutral atom in experiments. A straightforward solution is to directly produce single photons via a number of atoms. We theoretically investigate such a single-photon emitter in which a bunch of Sr atoms are tightly confined in a blue-detuned optical lattice and weakly driven by an external field. The strong long-range interatomic interactions inducing large excitation-energy shifts results in a significant suppression of multiphoton emission. We consider two common approaches, which are widely used in experiments to generate single photons, in detail. The results indicate a potential to built up a single-photon source based on an ensemble of interacting atoms.

DOI: 10.1103/PhysRevA.89.063809 PACS number(s): 42.50.Ar, 42.50.Ct, 42.50.Dv, 42.50.Pq

## I. INTRODUCTION

A single-photon source [1], which deterministically delivers one single quantum of light at a time, is particularly valuable in quantum information processing, since single photons act as qubits storing information in their polarization state or phase [2]. This encoding scheme has been maturely used to establish identical random binary numbers (quantum keys) at remote locations in the quantum cryptography [3] and has an ambitious photonic application in the linear optical quantum computing [4].

Several novel schemes, which can be potentially applied to work as a single-photon source, have been experimentally demonstrated based on a variety of individual two-state particles, such as an atom [5], an ion [6], a molecule [7], and a quantum dot [8]. An individual two-state particle emitting single photons arises from the fact that it takes some time for the driving field to reexcite the damped particle so as to emit the next photon. However, the single-photon generation is strongly influenced by the particle-number fluctuations in experiments, since it is a tough task to isolate a single particle, especially a neutral atom, from a large number of samples [9–11]. Therefore exploiting a single-photon emitter based on a number of neutral atoms is necessary and meaningful in both theoretical and experimental aspects.

At present, a single-photon emitter based on the effect of a Rydberg blockade [12] has been becoming more and more attractive, since it provides a straightforward way to probe the nature of the interatomic interactions through the emitted photons and, in particular, generate single photons from a multiatom system. The excitation blockade effect, which results from the interatomic interactions shifting the energy levels of Rydberg atoms, strongly weakens the simultaneous excitation of two or more atoms, and hence the multiphoton absorption is significantly suppressed. As a result, a bunch of Rydberg atoms scatter the driving-field photons one by one [13].

Similar to the excitation blockade in Rydberg atoms, the strong long-range interatomic interactions induced by exchanging virtual photons between identical atoms also cause large excitation-energy shifts [14], which results in the suppression of both atomic excitation and multiphoton processes. In Ref. [15], the author has proven that the fluorescence antibunched photons emitted from an ensemble of strongly interacting Sr atoms, which are tightly confined in a blue-detuned optical lattice, in the low-excitation limit. This is because for a weak driving strength the ensemble of coupled atoms can be simplified as a two-state "particle" in the Hilbert space [16] and the fluorescence photons are mainly from several super-radiant–spontaneous–emission modes. In the spirit of such an interaction-induced photon antibunching effect, we present here an experimentally feasible scheme of a single-photon emitter based on the platform established in Ref. [15], which can be potentially improved to work as a single-photon source.

We consider two common approaches, i.e., a cavity emitter driven by a continuous laser field [17] and a pulse-driven emitter without optical resonator [18], which are usually applied in experiments to generate single photons. Each method has both advantages and disadvantages. The spatial mode of a single photon's output from a cavity emitter is well defined and the photon polarization is unique [19]. However, photons are emitted at random times and not deterministically due to the weak atom-cavity interaction and continuous driving. In contrast, a pulse-triggered emitter in free space (without cavity) generates the single fluorescence photons deterministically with the arrival times depending on the excited-state lifetime and the pump-pulse duration [18]. However, the highly efficient collection of the "triggered" fluorescence, which is directed into the full solid angle, is still a challenge in experiments [20].

In this paper we focus on the dependence of the second-order correlation of the photon emission, which is a key diagnostic of the nonclassical nature of the light, on different system parameters in detail as well as the temporal coherence of single photons. Our physical system offers a prospect for realizing a single-photon source based on a bunch of interacting neutral atoms.

## II. A CAVITY EMITTER DRIVEN BY A CONTINUOUS LASER FIELD

We firstly consider a cavity emitter, where a bunch of continuous-field–driven atoms are placed inside an optical

*Deshui.Yu@nottingham.ac.uk

 

resonator. The single photon's output from such an emitter has a well-defined spatial mode and unique polarization.

### A. Physical model

An ensemble of $N$ bosonic Sr atoms is tightly confined in a two-dimensional (2D) blue-detuned hexagonal optical lattice operating at a magic wavelength of $\lambda_b = 412.8$ nm [21]. The 2D hexagonal lattice [22] is formed in the $y-z$ plane and Sr atoms are arranged along the $z$ direction, with each lattice site containing only one atom, as shown in Fig. 1. Since the nearest-neighbor distance, i.e., the lattice constant $a = \frac{4}{3\sqrt{3}}(\frac{\lambda_b}{2})$, is much shorter than the atomic $(5s5p)^3P_0 - (5s4d)^3D_1$ transition wavelength ($\lambda_a \simeq 2.6$ $\mu$m), the strong anisotropic long-range dipolar interactions, which can extend over a few lattice sites, and the collective dissipation can be induced in the atomic ensemble via exchanging virtual photons among atoms [14]. We should illustrate that the reason for applying the 2D hexagonal lattice rather than the common one-dimensional lattice [15] is that even a small reduction of the nearest-neighbor distance can strongly enhance the interatomic interactions, since the dipole-dipole interaction is proportional to the inverse third power of the separation of two atoms.

An external monochromatic field $\mathbf{E}_p$, which propagates along the $x$ axis and whose polarization $\hat{\mathbf{e}}_p$ is in the $z$ direction, is applied to excite atoms from $|g\rangle \equiv (5s5p)^3P_0$ to $|e\rangle \equiv (5s4d)^3D_1(m=0)$ with the atom-field detuning $\Delta \equiv \omega_p - \omega_a$ (the coupling field frequency $\omega_p$ and the atomic $|g\rangle - |e\rangle$ transition frequency $\omega_a$) and Rabi frequency $\Omega = -dE_0/(2\hbar)$. Here $d \simeq 4.04$ Debye [21] is the electric-field-induced dipole moment corresponding to the atomic $(5s5p)^3P_0 - (5s4d)^3D_1$ transition and $E_0$ is the amplitude of the coupling laser field $\mathbf{E}_p$.

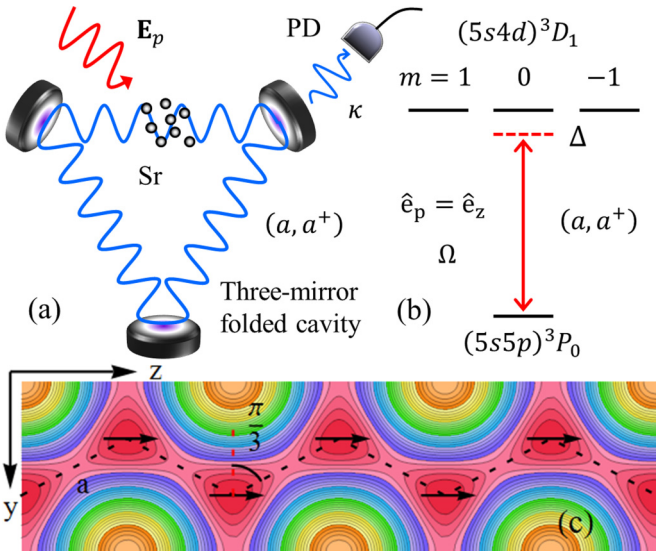


FIG. 1. (Color online) Schematic of a laser-driven atom-cavity system. (a) A single-mode folded cavity couples to an ensemble of Sr atoms. ($a$,$a^+$) are the annihilation and creation operators for the cavity mode, respectively, and $\kappa$ is the cavity damping rate. A photodetector (PD) is placed outside the cavity to measure the output photons. An external laser field $\mathbf{E}_p$ polarized in the $z$ direction and propagating along the $x$ axis is applied to couple the atomic $(5s5p)^3P_0 - (5s4d)^3D_1(m=0)$ transition with a Rabi frequency $\Omega$, as shown in (b). Both the cavity mode and external driving field have the same frequency $\omega_p$ and the atom-field detuning is defined as $\Delta = \omega_p - \omega_a$. (c) Sr atoms are tightly confined in a blue-detuned hexagonal optical lattice created by three laser beams intersecting in the $y-z$ plane. The lattice constant is $a = \frac{4}{3\sqrt{3}}(\frac{\lambda_b}{2})$.

In order to efficiently control the spatial mode and polarization of photons emitted from the atomic ensemble, all Sr atoms are localized inside a single-mode traveling-wave optical resonator [23] with the cavity-mode frequency being equal to $\omega_p$. The intracavity photons propagate along the $y$ direction and the corresponding photon loss rate is $\kappa$. The creation and annihilation operators of the cavity mode are $a$ and $a^+$, respectively, and the atom-cavity coupling strength is $g$. An ideal photodetector is used to measure the output photons leaking through the resonator mirror.

Since the branching ratio of the atomic $(5s5p)^3P_0 - (5s4d)^3D_1$ transition, of whom the spontaneous emission rate is about $\gamma = 2\pi \times 46.18$ kHz, nearly reaches 60% of the total decay rate of the $(5s4d)^3D_1$ level [24], our Sr lattice can be approximately considered as an open quantum system comprised of two-level particles being simultaneously coupled to an external laser field and an optical cavity.

### B. Dissipative quantum dynamics

The dissipative dynamics of an ensemble of laser-driven Sr atoms being coupled to an optical cavity can be described by the master equation

$$\dot{\rho} = -\frac{i}{\hbar}[H,\rho] + \mathcal{D}(\rho), \tag{1}$$

where $\rho$ is the combined atom-cavity field density operator. The Hamiltonian $H$ describing the coherent time evolution of the open quantum system is expressed as

$$H = -\hbar\sum_{\alpha}\Delta b_\alpha^+ b_\alpha + \hbar\sum_{\alpha,\beta\neq\alpha} V_{\alpha,\beta} b_\alpha^+ b_\beta - \hbar\sum_{\alpha}\left[b_\alpha^+\left(\Omega e^{i\mathbf{k}_p\cdot\mathbf{r}_\alpha} + g a e^{i\mathbf{k}_c\cdot\mathbf{r}_\alpha}\right) + \text{H.c.}\right], \tag{2}$$

where the coefficient

$$V_{\alpha,\beta} = \frac{3\gamma}{4}\left[-(1-\cos^2\theta_{\alpha,\beta})\frac{\cos\eta_{\alpha,\beta}}{\eta_{\alpha,\beta}} + (1-3\cos^2\theta_{\alpha,\beta})\left(\frac{\sin\eta_{\alpha,\beta}}{\eta_{\alpha,\beta}^2} + \frac{\cos\eta_{\alpha,\beta}}{\eta_{\alpha,\beta}^3}\right)\right] \tag{3}$$

characterizes the long-range coherent interaction between the $\alpha$th and $\beta$th atoms with the relative position vector $\mathbf{r}_{\alpha,\beta} \equiv \mathbf{r}_\alpha - \mathbf{r}_\beta$. $b_\alpha \equiv (|g\rangle\langle e|)_\alpha$ is the atomic transition operator for the $\alpha$th atom; $\mathbf{k}_p$ and $\mathbf{k}_c$ are the wave vectors of the coupling field $\mathbf{E}_p$ and cavity mode, respectively; and here we have defined the dimensionless parameter $\eta_{\alpha,\beta} = 2\pi|\mathbf{r}_{\alpha,\beta}|/\lambda_a$. $\theta_{\alpha,\beta}$ is the angle between the light-induced-dipole vector and $\mathbf{r}_{\alpha,\beta}$. The dissipation term $\mathcal{D}(\rho)$ in Eq. (1), which describes the collective spontaneous emission of the excited atoms and

photons escaping the optical cavity, takes the Lindblad form

$$\mathcal{D}(\rho) = \sum_{\alpha,\beta} \frac{R_{\alpha,\beta}}{2}(2b_\alpha \rho b_\beta^+ - b_\alpha^+ b_\beta \rho - \rho b_\alpha^+ b_\beta) + \frac{\kappa}{2}(2a\rho a^+ - a^+ a\rho - \rho a^+ a), \quad (4)$$

where the strength of dissipative coupling between two atoms is given by

$$R_{\alpha,\beta} = \frac{3\gamma}{2}\left[(1-\cos^2\theta_{\alpha,\beta})\frac{\sin\eta_{\alpha,\beta}}{\eta_{\alpha,\beta}} + (1-3\cos^2\theta_{\alpha,\beta})\left(\frac{\cos\eta_{\alpha,\beta}}{\eta_{\alpha,\beta}^2} - \frac{\sin\eta_{\alpha,\beta}}{\eta_{\alpha,\beta}^3}\right)\right]. \quad (5)$$

To understand the effect of collective spontaneous emissions in the quantum dynamics, we rewrite the dissipation term $\mathcal{D}(\rho)$ in diagonal form

$$\mathcal{D}(\rho) = \sum_{m=1}^{N} \frac{\gamma_m}{2}(2J_m \rho J_m^+ - J_m^+ J_m \rho - \rho J_m^+ J_m) + \frac{\kappa}{2}(2a\rho a^+ - a^+ a\rho - \rho a^+ a), \quad (6)$$

where $J_m = \sum_\alpha M_{m,\alpha} b_\alpha$ is the collective quantum jump operator and $\gamma_m = \sum_{\alpha,\beta} M_{m,\alpha} R_{\alpha,\beta} M_{\beta,m}^+$ is the corresponding collective decay rate. Here we assume that $\{\gamma_m, m = 1, \ldots, N\}$ have been already arranged from the minimum to the maximum. The transformation matrix $\mathbf{M} = (M_{m,\alpha})$ is composed of eigenvectors of the square matrix $\mathbf{R} = (R_{\alpha,\beta})$. Finally, one can represent $H$ in terms of $J_m$ and $J_m^+$,

$$H = -\hbar \sum_{m,n} V'_{m,n} J_m^+ J_n - \hbar \sum_m (\Omega_m J_m^+ + \Omega_m^* J_m) - \hbar \sum_m (g_m J_m^+ a + g_m^* a^+ J_m), \quad (7)$$

where $V'_{m,n} = \sum_{\alpha,\beta} M_{m,\alpha} V_{\alpha,\beta} M_{\beta,n}^+ - \Delta\delta_{m,n}$, $\Omega_m = \Omega \sum_\alpha M_{m,\alpha} e^{i\mathbf{k}_p\cdot\mathbf{r}_\alpha}$, and $g_m = g \sum_\alpha M_{m,\alpha} e^{i\mathbf{k}_c\cdot\mathbf{r}_\alpha}$. The diagonal matrix elements $V'_{m,m}$ correspond to the excitation strengths induced by interatomic interactions, while the nondiagonal elements $V'_{m,n}$ indicate the coupling strengths between different collective quantum jump modes. Here we apply the Monte Carlo wave function (MCWF) approach [25] to numerically solve the master equation (1).

### C. Intracavity photon-number and photon-antibunching effect for a system with $N = 2$

We focus on two experimentally measurable quantities, i.e., the expectation values of the photon number

$$N_p \equiv \langle a^+(t)a(t)\rangle_{t\to\infty} \quad (8)$$

and the second-order correlation function

$$g^{(2)}(\tau) \equiv \frac{\langle a^+(t)a^+(t+\tau)a(t+\tau)a(t)\rangle_{t\to\infty}}{\langle a^+(t)a(t)\rangle_{t\to\infty}^2} \quad (9)$$

of intracavity photons in the stationary (denoted by $t \to \infty$) state of the open quantum system and investigate their dependence on the experimentally tunable parameters $\Omega$, $\Delta$, $\kappa$, and $g$. The definition of $g^{(2)}(\tau)$ corresponds to the measurement of the Hanbury Brown–Twiss (HBT) setup and characterizes the photon statistics of light sources. For an ideal single-photon emitter, $g^{(2)}(\tau)$ minimizes in the short delay time limit $g^{(2)}(\tau = 0) = 0$.

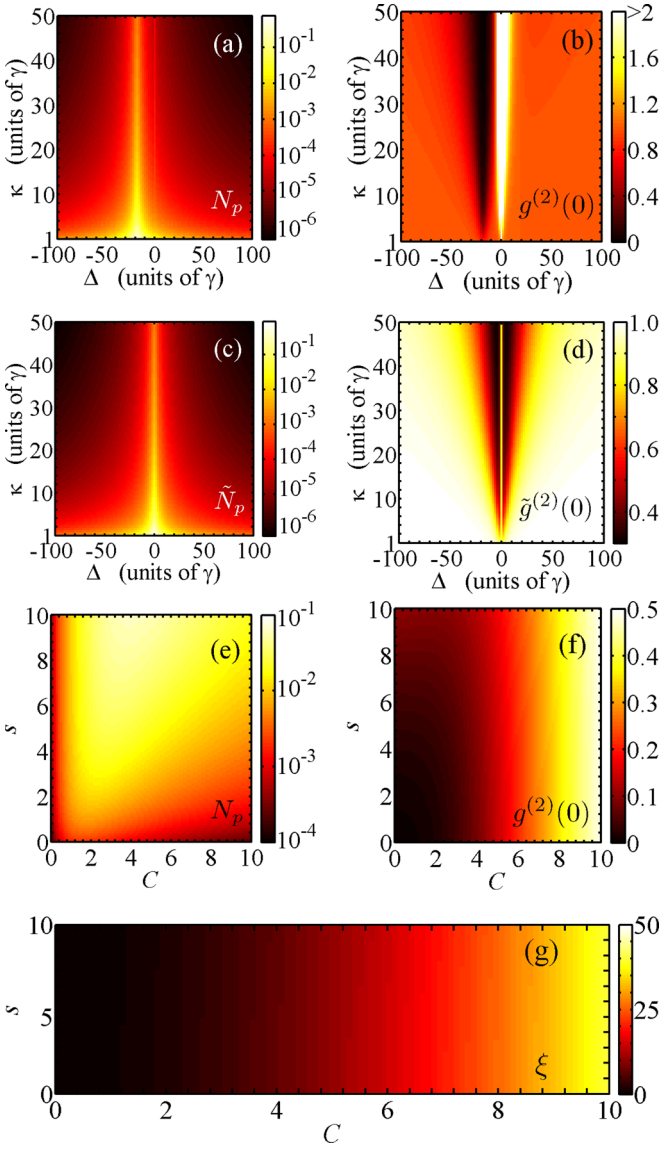


FIG. 2. (Color online) The dependence of intracavity field intensity $N_p$ and the second-order correlation function $g^{(2)}(\tau)$ at $\tau = 0$ on parameters $\Omega$, $\Delta$, $\kappa$, and $g$ for a two-atom system. (a) $N_p$ as a function of $\kappa$ and $\Delta$ for $\Omega = g = \gamma$. The corresponding $g^{(2)}(0)$ is shown in (b). For comparison, $\tilde{N}_p$ and $\tilde{g}^{(2)}(0)$ for a noninteracting system with $V_{\alpha,\beta} = 0$ and $R_{\alpha,\beta} = \gamma\delta_{\alpha,\beta}$ are displayed in (c) and (d), respectively. (e) $N_p$ changing with the saturation parameter $s$ and the cooperativity parameter $C$ for $\Delta = -18\gamma$ and $\kappa = 50\gamma$. The corresponding $g^{(2)}(0)$ is displayed in (f). (g) The ratio $\xi$ of the intracavity photons leaving the cavity to the fluorescence photons from the spontaneous emission.

First, we consider a simple system with $N = 2$, the results of which can give us some instructions for the analog larger systems. Figure 2(a) displays $N_p$ as a function of $\Delta$ and $\kappa$ for a pair of fixed $\Omega$ and $g$, and the corresponding dependence of $g^{(2)}(\tau)$ at $\tau = 0$ is shown in Fig. 2(b). For comparison, we also display $\tilde{N}_p$ and $\tilde{g}^{(2)}(\tau = 0)$ for a system composed

of independent atoms, i.e., $V_{\alpha,\beta}=0$ and $R_{\alpha,\beta}=\gamma\delta_{\alpha,\beta}$, in Figs. 2(c) and 2(d), respectively. As one can see, reducing the cavity loss rate $\kappa$ can enhance the intracavity field intensity $N_p$. Additionally, unlike $\tilde{N}_p$, $N_p$ does not maximize at the resonant atom-field coupling for a fixed $\kappa$ but at the detuning $\Delta=V_{1,2}$, which results from the interaction-induced excitation-energy shift [15].

Interestingly, at $\Delta=V_{1,2}$, $g^{(2)}(\tau=0)$ fails to a value very close to zero as $\kappa$ is increased, which indicates the strong photon antibunching effect occurs in the bad-cavity limit $\kappa\gg\gamma$. Conversely, bunched photons, i.e., $g^{(2)}(\tau=0)>1$, leak from the output cavity mirror for the resonant atom-cavity interaction $\Delta=0$ [see Fig. 2(b)]. For a noninteracting system, although the photon antibunching emission happens in the off-resonance region $\Delta\neq 0$, the minimum of $\tilde{g}^{(2)}(\tau=0)$ is strongly enhanced compared with that of $g^{(2)}(\tau=0)$ [see Fig. 2(d)] due to two atoms independently emitting photons.

Two factors contribute to the strong photon antibunching effect in an interacting system: (i) Due to the large excitation-energy shifts induced by the strong interatomic interactions, the multiphoton absorption is strongly suppressed, i.e., the drive-field photons can be absorbed and scattered only one by one [15]. (ii) Due to the large damping rate of the cavity, once a photon is scattered from the driving field into the cavity mode, it rapidly escapes from the optical resonator. As a result, there is less than one photon traveling inside the cavity.

In order to look into the cooperative effects of the atom-driving-field interaction and the atom-cavity field coupling on $N_p$ and $g^{(2)}(\tau=0)$ in detail, here we define the on-resonance saturation parameter $s=\Omega^2/\gamma^2$ and the cooperativity parameter per atom $C=g^2/(\kappa\gamma)$ and consider their relations to the intracavity photons. For a pair of fixed $\Delta$ and $\kappa$, the strong driving field, i.e., $s>1$, gradually raises the intracavity intensity $N_p$ and reduces the photon antibunching effect, since the larger Rabi frequency enhances the multiphoton transition. For an ensemble of strongly interacting atoms, $s$ can vary in a wide range with $g^{(2)}(\tau=0)$ maintaining a small value. In addition, for a weak atom-cavity interaction, increasing $C$ is good at converting the external field $\mathbf{E}_p$ into the cavity mode. However, intracavity photons can be reabsorbed by atoms for a large $C$, which vanishes in the intracavity field, as shown in Fig. 2(c). Moreover, enhancing the atom-cavity coupling weakens the photon antibunching effect.

Here we define a parameter $\xi$ to describe the ability of the spontaneously emitted photons being converted into the intracavity field,

$$\xi=\frac{\kappa\langle a^{+}(t)a(t)\rangle_{t\to\infty}}{\sum_m\gamma_m\langle J_m^{+}(t)J_m(t)\rangle_{t\to\infty}},\tag{10}$$

where the numerator denotes the loss rate of intracavity photons and the denominator gives the total spontaneous emission rate of atoms. As shown in Fig. 2(g), the loss rate of the intracavity field well exceeds the spontaneous emission of atoms, which means the intracavity photons are mainly from the atoms elastically scattering the driving field into the cavity mode rather than the spontaneously emitted photons. Increasing the atom-cavity coupling strongly suppresses the effect of the atomic spontaneous emission on the intracavity field, which corresponds to the case of cavity QED in the strong-coupling limit [26]. In addition, $\xi$ depends less on the atom-field saturation parameter $s$.

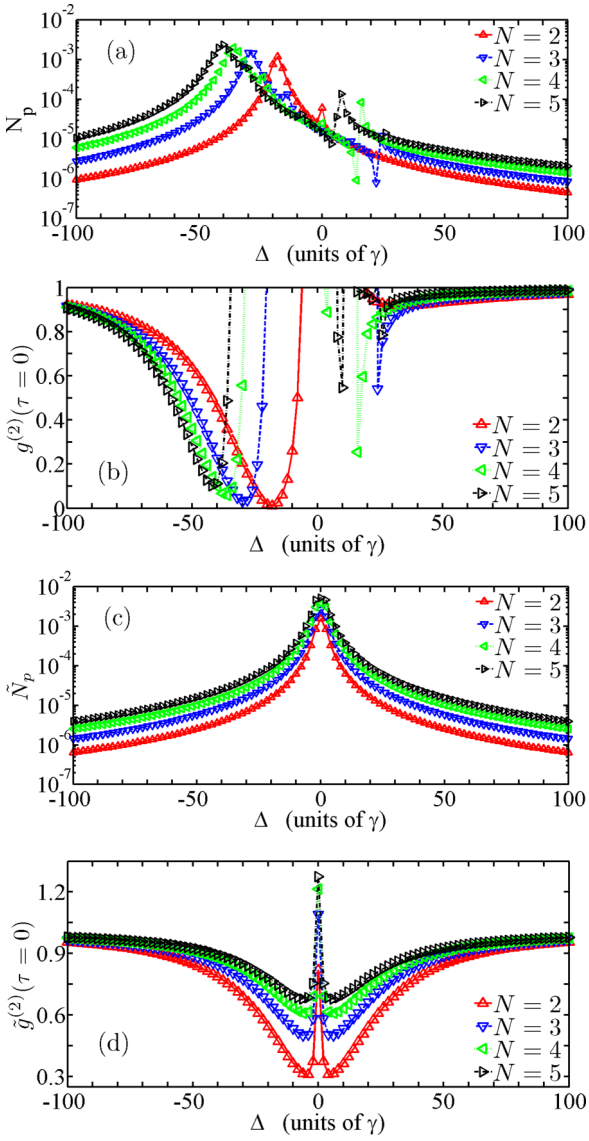


FIG. 3. (Color online) $N_p$ and $g^{(2)}(\tau=0)$ as a function of $\Delta$ for several different numbers of atoms are displayed in (a) and (b), respectively. For comparison, $\tilde{N}_p$ and $\tilde{g}^{(2)}(\tau=0)$ for the noninteracting system are shown in (c) and (d), respectively. For all curves, $\kappa=50\gamma$, $s=1$, and $C=0.02$.

### D. Single-photon emitters with $N>2$

Above we have systematically investigated a system composed of two atoms. Now we consider systems with $N>2$. Figure 3 illustrates $N_p$ and $g^{(2)}(\tau=0)$ changing with $\Delta$ for several different atomic numbers $N$ in the bad-cavity ($\kappa\gg\gamma$) and weak-coupling ($C\ll 1$) limit. For comparison, we also display the corresponding $\tilde{N}_p$ and $\tilde{g}^{(2)}(\tau=0)$ for the noninteracting systems in Fig. 3. As one can see, the detuning $\Delta$, at which the intracavity photon number $N_p$ maximizes, approaches to the summation of all interatomic interactions, i.e., $\sum_\beta V_{\alpha,\beta}$, for an arbitrary $\alpha$th atom as $N$ is increased, whereas the maximum of $\tilde{N}_p$ always happens

TABLE I. Collective decay rates $\gamma_m$, collective coupling strengths $\Omega_m$, and collective atom-cavity interactions $g_m$ for a system composed of $N = 5$ atoms.

| $m$ | 1 | 2 | 3 | 4 | 5 |
|---|---|---|---|---|---|
| $\gamma_m/\gamma$ | $4.0\times10^{-4}$ | $1.4\times10^{-3}$ | $1.8\times10^{-2}$ | 0.21 | 4.8 |
| $\Omega_m/\Omega$ | 0 | $3.5\times10^{-2}$ | $2.0\times10^{-2}$ | 0 | –2.2 |
| $g_m/g$ | 0 | $3.5\times10^{-2}$ | $2.0\times10^{-2}$ | 0 | –2.2 |

at the resonant atom-field interaction $\Delta = 0$. However, the interatomic interactions and collective dissipation have less affect on the maximum of intracavity photon number $N_p$ for different $N$ because less than one photon exists inside the cavity for the single-photon emission. Moreover, the photon antibunching effect is strongly enhanced in an interacting system compared with the corresponding noninteracting system. The minimum $g^{(2)}(\tau = 0)$ gradually rises when more atoms are placed inside the optical cavity, which is expected because the interaction-induced excitation-energy shifts are reduced as the system size is increased. Two atoms separated by a long distance scatter photons independently, which results in a reduced photon antibunching effect.

Without loss of generality, next we focus only on an open quantum system composed of $N = 5$ atoms, which is large enough to display the main features of an analogous larger system. As shown in Table I, the cooperative atom-field interactions $\Omega_{1,\ldots,4}$ and the collective atom-cavity coupling strengths $g_{1,\ldots,4}$ are much smaller than $\Omega_5$ and $g_5$, respectively. In addition, the collective decay rate $\gamma_5$ is almost 5 times larger than the intrinsic spontaneous emission rate $\gamma$ of a single atom, while the others are much smaller than $\gamma$ (see Table I).

In the Hilbert space for the atomic ensemble, a complete orthonormal basis can be chosen as $\{|\xi_1,\xi_2,\xi_3,\xi_4,\xi_5\rangle\}$, where the $\xi_\alpha$ state of the $\alpha$th atom can be either $|g\rangle$ or $|e\rangle$. This set of states can be divided into five groups, and all states in a certain group have the same number of excited atoms. For example, the single-excited-atom group is composed of $|e,g,g,g,g\rangle$, $|g,e,g,g,g\rangle$, $|g,g,e,g,g\rangle$, $|g,g,g,e,g\rangle$, and $|g,g,g,g,e\rangle$. Furthermore, one can apply the states in each group to compose the eigenstates of the interatomic-interaction term in Hamiltonian $\hbar\sum_{\alpha,\beta\neq\alpha} V_{\alpha,\beta} b_\alpha^\dagger b_\beta$. The corresponding eigenvalues denote the interatomic-interaction–induced energy shifts of different eigenstates. For example, the eigenvalue $E(G)$ for the ground state $|G\rangle = |g,g,g,g,g\rangle$ is zero and the single-excited-atom eigenstates are expressed as

$$\begin{pmatrix} |I,1\rangle \\ |I,2\rangle \\ |I,3\rangle \\ |I,4\rangle \\ |I,5\rangle \end{pmatrix} = W \begin{pmatrix} |e,g,g,g,g\rangle \\ |g,e,g,g,g\rangle \\ |g,g,e,g,g\rangle \\ |g,g,g,e,g\rangle \\ |g,g,g,g,e\rangle \end{pmatrix}, \tag{11}$$

where the square matrix $W$ is given by

$$W = \begin{pmatrix} 0.24 & -0.51 & 0.61 & 0.51 & 0.24 \\ 0.46 & -0.54 & 0.00 & 0.54 & -0.46 \\ -0.57 & 0.07 & 0.58 & 0.07 & -0.57 \\ -0.54 & -0.46 & 0.00 & 0.46 & 0.54 \\ 0.34 & 0.49 & 0.54 & 0.49 & 0.34 \end{pmatrix}, \tag{12}$$

with the corresponding eigenvalues $E(I,1) = 25.50\gamma$, $E(I,2) = 20.10\gamma$, $E(I,3) = 7.69\gamma$, $E(I,4) = -13.00\gamma$, and $E(I,5) = -40.30\gamma$. More details can be found in Ref. [15].

As shown in Fig. 3, the largest intracavity photon number and strongest photon antibunching happen at $\Delta \simeq -40\gamma$ for a five-atom interacting system, which exactly corresponds to the atomic $|G\rangle - |I,5\rangle$ transition. Consequently, by setting $\Delta \simeq -40\gamma$, the Hamiltonian (7) can be approximately written as

$$H \approx -\hbar(\Omega_5 + g_5 a)J_5^+ + \text{H.c.}, \tag{13}$$

and the dissipation term (6) is simplified as

$$\mathcal{D}(\rho) \approx \frac{\gamma_5}{2}(2J_5\rho J_5^+ - J_5^+ J_5\rho - \rho J_5^+ J_5) + \frac{\kappa}{2}(2a\rho a^+ - a^+ a\rho - \rho a^+ a) \tag{14}$$

in the weak-coupling limit, i.e., a two-state *particle* resonantly couples to an external driving field and a single-mode optical cavity simultaneously [15]. Next, we restrict ourselves in the bad-cavity limit $\kappa \gg \gamma$ and set $\Delta \simeq -40\gamma$, since the strong photon antibunching mainly occurs in this regime.

### E. Photon-number fluctuations

Besides the photon antibunching effect, i.e., $g^{(2)}(\tau = 0) < 1$, investigating the second-order correlation function $g^{(2)}(\tau)$ changing with the time delay $\tau$ is necessary since it is closely related to intensity fluctuations of the intracavity field. For a coherent laser field, $g^{(2)}(\tau)$ is expected to be unity for any $\tau$, which means the characteristic time scale of intensity fluctuations is infinite. For a thermal light, the characteristic damping time of $g^{(2)}(\tau)$ is determined by the temperature of the light source. For the fluorescence photons emitted from a single two-level atom, $g^{(2)}(\tau)$ can maintain a value smaller than unity during a time delay much longer than the excited-state lifetime in the weak-excitation limit, while the damping time of $g^{(2)}(\tau)$ is limited by the excited-state lifetime for the strong driving field.

The two-time correlation function $g^{(2)}(\tau)$ can be numerically investigated via the MCWF method [25]. Figure 4(a) illustrates the dependence of $g^{(2)}(\tau)$ on the time delay $\tau$ in a short-term scale. As one can see, $g^{(2)}(\tau)$ maintains a low value during a short time delay limited by $(2\gamma_5)^{-1}$, which means the atoms hardly emit the other photon into the cavity mode right after an intracavity photon escapes the optical resonator. It is understandable that the atomic ensemble is relatively overexcited after an intracavity photon leaving the cavity. Before atoms scatter the next driving-field photons into the cavity mode, the time scale of which is determined by $g^{-1}$, the atomic system undergoes a collective spontaneous emission with a rate of $\gamma_5$ ($\gg g$) and the spontaneously emitted photons do not match the cavity mode. After a short time delay $(2\gamma_5)^{-1}$, $g^{(2)}(\tau)$ grows dramatically as $\tau$ is increased. It is understandable that since less than one photon ($N_p \ll 1$) exists inside the optical resonator at a time, one photon being emitted into or leaving the cavity can induce large fluctuations in the number of intracavity photons, resulting in a steep rise of $g^{(2)}(\tau)$. Afterwards, $g^{(2)}(\tau)$ maintains the photon bunching

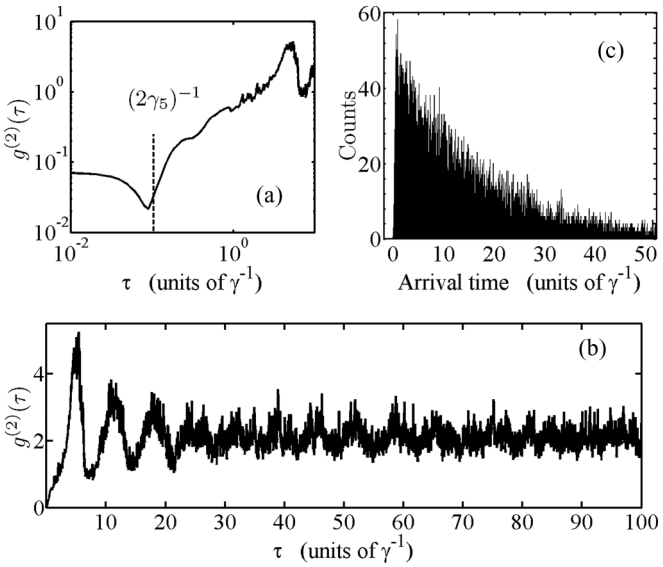


FIG. 4. (a) The second-order correlation function $g^{(2)}(\tau)$ as a function of the time delay $\tau$ in a short-term time scale. The dependence of $g^{(2)}(\tau)$ on $\tau$ in a wide range is shown in (b). (c) The corresponding distribution of photon arrival times numerically derived from the MCWF simulation. For all results, the system parameters are chosen to be $\Delta \simeq -40\gamma, \kappa = 50\gamma, s = 1$, and $C = 0.02$.

for a long time delay, as shown in Fig. 4(b). However, we can prove that $g^{(2)}(\tau)$ approaches unity finally.

Figure 4(c) displays a specific photon arrival-time interval distribution. One can see that the probability of photon arrival times strongly grows after a short time delay, which coincides with the behavior of $g^{(2)}(\tau)$ in the short time scale ($\tau < \gamma^{-1}$). Afterwards, the distribution of photon emission times decays exponentially with a rate parameter ($\kappa N_p$). Thus the characteristic time delay of $g^{(2)}(\tau)$ is given by $(\kappa N_p)^{-1}$. Since our single-photon emitter works in a low-emission-rate limit, the arrival time distributes over a wide time scale much longer than the excited-state lifetime $\gamma^{-1}$ of the atom. This indeterministic single-photon emission arises from the fact that the processes of atomic excitation and photon emission share the same atomic transition line, for which the nonclassical character of light only occurs in the weak-coupling limit ($C \ll 1$). By using a three-level [27,28] or four-level [29] atomic system, those two processes can be separated and the atom-cavity system can be adjusted to the strong-coupling limit ($C \gg 1$), with the photon antibunching effect being maintained. As a result, the photon arrival time can be greatly reduced.

### F. The first-order correlation

So far, we have discussed only the second-order correlation function $g^{(2)}(\tau)$. However, it is not the whole story, since the emergence of various photonic applications requires the emitted single photons possess high coherence. Thus it is necessary to consider the temporal optical coherence of photons, which is described by the first-order correlation function

$$g^{(1)}(\tau) \equiv \frac{\langle a^+(t+\tau)a(t)\rangle_{t\to\infty}}{\langle a^+(t)a(t)\rangle_{t\to\infty}}. \tag{15}$$

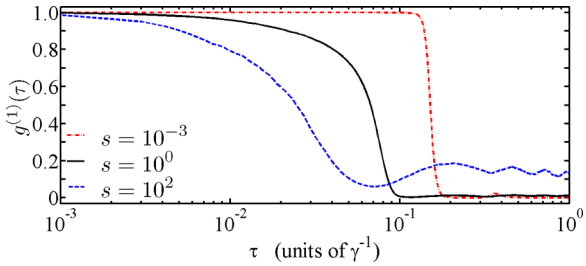


FIG. 5. (Color online) The first-order correlation $g^{(1)}(\tau)$ as a function of the time delay $\tau$ with $\Delta = -40\gamma$ and $C = 0.02$. Two distinct regions with $g^{(1)}(\tau) \simeq 1$ and $g^{(1)}(\tau) \simeq 0$, respectively, can be distinguished in the limit of weak atom-field interaction $s \simeq 0$. The boundary is given by $\gamma_5^{-1}$ in the time domain.

For the resonance fluorescence from an individual quantum emitter without an optical resonator [6,7], the spontaneous emission rate $\gamma$ mainly limits the spectral linewidth for a large driving strength. Conversely, the subnatural-linewidth single photons are generated from a single quantum emitter working in the Heitler regime [30]. However, the situation can be considerably altered if the object is placed inside an optical cavity. Again, we apply the MCWF procedure [25] to numerically calculate the two-time correlation function $g^{(1)}(\tau)$, and the results for different saturation parameters $s$ are displayed in Fig. 5.

As one can see, $g^{(1)}(\tau)$ displays two distinct regions, i.e., one region with extremely high coherence [$g^{(1)}(\tau) \simeq 1$] and the other with noncoherence [$g^{(1)}(\tau) \simeq 0$], divided by the collective spontaneous emission time $\gamma_5^{-1}$ in the time domain. The boundary between these two regions becomes more obvious as the atom-field interaction approaches zero, $s \sim 0$. This dependence of $g^{(1)}(\tau)$ on $\tau$ can be understood from the large photon-number fluctuations in the intracavity field.

As is known, both intensity and phase fluctuations of intracavity field contribute to the decay of $g^{(1)}(\tau)$. For the conventional lasers, an optical cavity is filled with a macroscopical number of photons. In this case, the intensity fluctuations (fluctuations in the number of intracavity photons) has less influence on the first-order correlation of the laser field, while the field phase diffusion, which is mainly induced by the unavoidable spontaneous emission of emitters, primarily contributes to the linewidth of the laser spectrum. However, the situation is very different in our system, since the stimulated emission, which is particularly important in the lasing process, is significantly suppressed in the weak-excitation limit and the intracavity field is mainly from the atoms elastically scattering the driving field into the cavity mode.

In our single-photon emitter, less than one photon exists simultaneously inside the optical resonator at any time due to the large loss rate $\kappa$. A single-photon change inside the cavity can induce large photon-number fluctuations, resulting in a dramatic influence on the intracavity field coherence. As shown in Fig. 4(a), the intracavity field undergoes relative small fluctuations in photon number in a short time delay $\gamma_5^{-1}$. In this time scale, the field phase fluctuations mainly determine $g^{(1)}(\tau)$. Since the collective coupling strength $\Omega_5$ is much smaller than the corresponding collective decay rate $\gamma_5$, i.e., the Heitler regime [30], in the limit of $s \sim 0$, the

intracavity field correlation is mainly determined by the driving field in this time scale, which results in $g^{(1)}(\tau) \sim 1$. In contrast, for a relatively long time delay $\tau > \gamma_5^{-1}$, the system suffers from huge photon-number fluctuations [see Fig. 4(a)], which extremely reduces the first-order correlation (see Fig. 5).

## III. A SINGLE-PHOTON EMITTER IN A PULSED FASHION

So far, we have discussed a single-photon emitter based on interacting neutral atoms driven by a continuous-wave laser field and coupled to an optical resonator. The single photons emitted from such a physical system have a well-defined spatial mode and polarization. However, the photon emission rate is very low (see Fig. 3) and single photons are created at random times [see Fig. 4(c)] due to the weak atom-cavity coupling and the continuous pumping. Additionally, the temporal coherence of single photons is strongly affected by the huge photon-number fluctuations.

In order to generate single photons deterministically, a control of the emission process is necessary. In experiments, a rectangular optical pulse is usually applied to excite a single absorber with probability 1 and, subsequently, a single photon is produced via the spontaneous emission. Hence we next consider a single-photon emitter triggered by excitation pulses. Moreover, to avoid the strong fluctuations in the number of intracavity photons induced by the weak atom-cavity coupling, the pulse-driven lattice-confined Sr atoms are localized in the free space (without optical resonator), as shown in Fig. 6. The fluorescence photons are collected by a lens (here we assume a 100% photon collection efficiency) and the second-order temporal correlation function is measured via a HBT-type setup composed of a beam splitter and two photon-counting detectors.

### A. Deterministic single-photon emission

Again, we focus on an interacting system composed of $N = 5$ atoms, which are excited by the rectangular pulses polarized in the $z$ axis and propagating along the $y$ direction. We still apply the master equation [Eq. (1)] to investigate the system dynamics, except deleting all the terms related to the optical cavity in the Hamiltonian [Eq. (7)] and dissipation [Eq. (6)]. As discussed in the last section, due to the large interaction-induced energy shifts, the complex quantum system in the coupled representation can be simplified as a two-state particle resonantly interacting with an external laser field with a collective driving strength $\Omega_5$ in the low-excitation

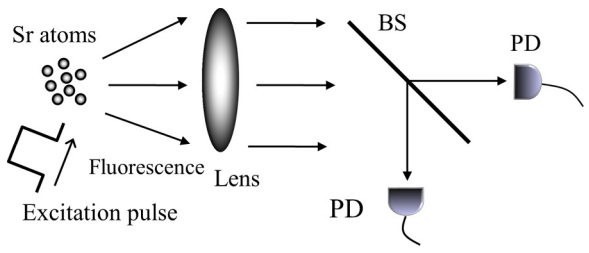


FIG. 6. Schematic of a triggered single-photon emitter. A bunch of lattice-confined atoms are excited by rectangular laser pulses. A lens is applied to collect the fluorescence light, which is separated by a beam splitter (BS) and imaged onto two photodetectors (PD).

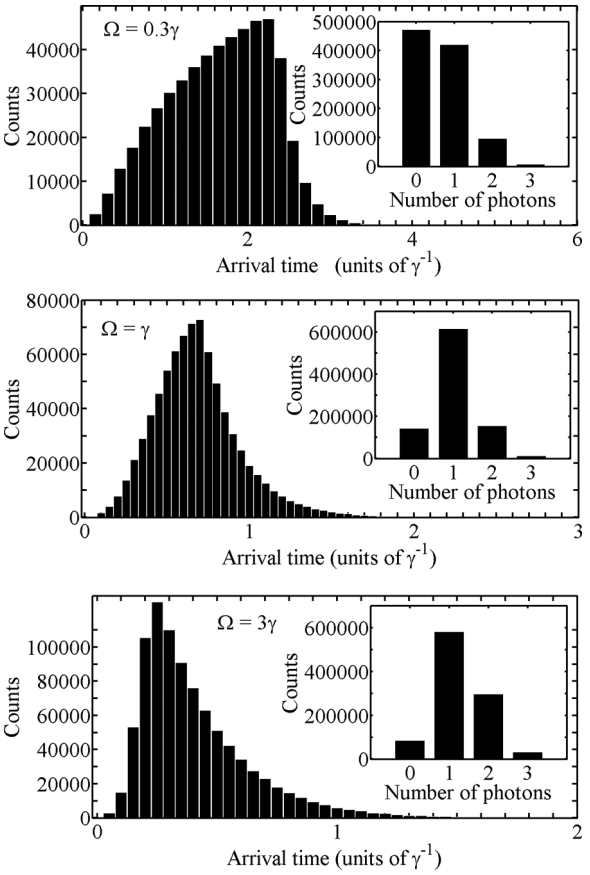


FIG. 7. The arrival times of fluorescence photons recorded with one photodetector for several different driving strengths Ω. The atom-field detuning is fixed at $\Delta = -40\gamma$, and the pulse duration is set to be $\tau_p = \frac{\pi}{2\Omega_5}$. The insets show the corresponding histograms of the number of photons emitted by one excitation pulse.

limit when the global atom-field detuning is set at $\Delta \simeq -40\gamma$. Moreover, it has been shown in Ref. [31] that the optimal choice for a single-photon emitter based on a two-level atom is to apply $\pi$ pulses. Therefore here we set the excitation-pulse area to satisfy the condition

$$2\Omega_5\tau_p = \pi, \tag{16}$$

where $\tau_p$ is the excitation-pulse duration.

We first prove that the setup described in Fig. 6 deterministically produces photons for an excitation pulse. Figure 7 displays the statistical distribution of the arrival times of emitted fluorescence photons for one trigger pulse with different durations $\tau_p$. As one can see, the photon emission strongly rises during the pulse duration and is maximized at the end of the pulse. Afterwards, the distribution decays exponentially with a time constant of $\gamma_5^{-1}$. In this case, single photons are generated at predetermined times within a scale of $\tau_p + \gamma_5^{-1}$. By efficiently reducing the excitation duration $\tau_p$, the time scale for generating single photons is completely limited by the quantum system itself. In addition, a two-level absorber with a large spontaneous emission rate can narrow the distribution of predetermined times. However, the temporal coherence of single photons is strongly reduced, since the radiation field is totally from the spontaneous emission.

Having checked that photons are generated deterministically, we should determine the number of photons emitted from the system triggered by a single excitation pulse. The numerical results are shown in the insets of Fig. 7, which clearly illustrate the efficiency of producing single photons can exceed 60%. The probability of single photon generated by one excitation pulse is strongly dependent on the $\pi$-pulse intensity (or duration). On one hand, reducing the $\pi$-pulse intensity is an efficient way to suppress the multiphoton emission, but the probability of a vacuum state (no photon emission) rises dramatically since the atomic system will hardly be excited at a small $\Omega_5$. On the other hand, the multiphoton processes are enhanced as the $\pi$-pulse intensity is increased and exceed any interaction-induced energy shifts. Therefore the $\pi$-pulse duration needs to be carefully chosen so as to optimize the single-photon generation. Moreover, enhancing the interatomic interactions via reducing the atomic spacing is a useful way to suppress the probabilities of both vacuum state and multiphoton emission.

### B. Time-resolved coincidence

In order to give a complete description of the nonclassical statistics of our single-photon emitter, we consider the second-order correlation function of the fluorescence photons emitted from a system being continuously excited by a sequence of $\pi$ pulses with a fixed period, which is much larger than the collective decay time $\gamma_5^{-1}$.

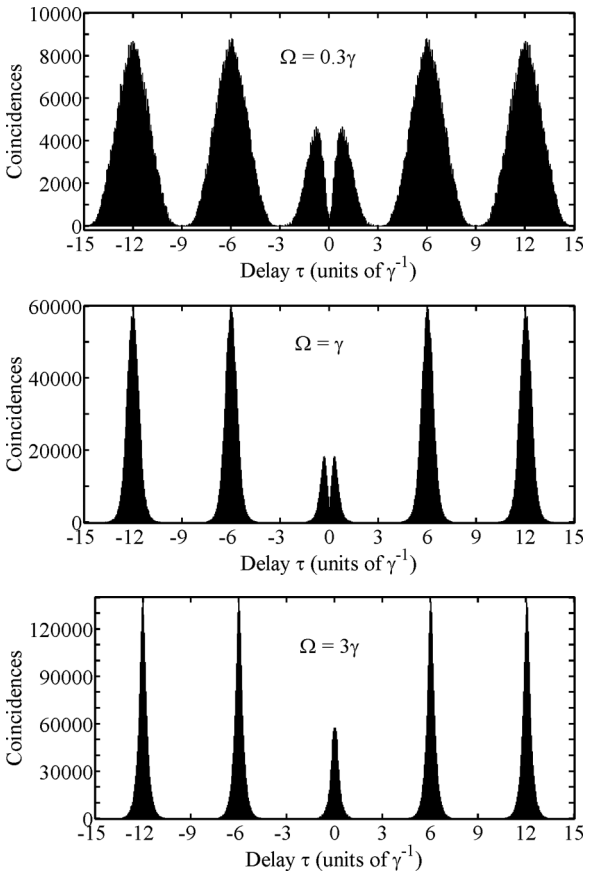


FIG. 8. Photon correlation histogram of the photon emission for different Rabi frequencies $\Omega$. The area of each excitation pulse is fixed at $2\Omega_5\tau_p = \pi$ and the repetition rate is set to be $6\gamma$. Since the photon emission time is determined by $\tau_p + \gamma_5^{-1}$, shortening the pulse duration $\tau_p$ can narrow the $1/e$ half-width of peaks of the correlation histogram but enhance the two-photon emission.

We numerically derive the number of coincidence photon-emission events as a function of time delay $\tau$ via the MCWF simulation. Figure 8 displays the resulting histogram, from which one can see a series of spikes separated by the period of the excitation pulses. The signature of single-photon emission is evident in the strongly reduced central peak, which indicates the significant suppression of the two-photon emission at $\tau = 0$. The $1/e$ half-width of the peaks is determined by the summation of the pulse duration $\tau_p$ and the collective lifetime $\gamma_5^{-1}$.

The height of the central peak grows when the $\pi$-pulse duration is shortened because the enlarged Rabi frequency exceeds the interaction-induced energy shifts of different excitation levels and induces multiphoton emissions. In contrast, the central peak is suppressed as the $\pi$-pulse duration is extended, which results from the inhibition of multiphoton processes.

Figure 8 proves the deterministic generation of single photons from a number of interacting atoms. Reducing the interatomic distance, which results in enhancing the interaction strength between atoms, can maintain the single-photon generation for a system composed of more atoms because of the enlarged excitation-energy shifts [15]. This result is very meaningful in experiments, since it is difficult to prepare the single neutral atom from a large number of samples [9].

## IV. SUMMARY

In conclusion, we have systematically studied a single-photon emitter based on the interaction-induced photon antibunching effect [15]. We focus on two common approaches, i.e., a cavity emitter continuously driven by an external light field and an emitter composed of pulse-driven atoms in free space, applied usually in experiments to generate single photons. Each method has distinguishing features.

For a cavity emitter, an ensemble of interacting atoms is localized inside a bad optical resonator ($\kappa \gg \gamma$) and illuminated by a continuous-wave light. Due to the weak coupling between atoms and cavity ($C \ll 1$), atoms inefficiently convert the driving field into the cavity mode, which leads to a low single-photon emission rate and large fluctuations in the intracavity photon number. As a result, the temporal coherence of single photons is restricted by huge photon-number fluctuations. This weakness can be overcome by separating the excitation and emission processes by using different transition lines [27–29]. In this case, the atom-cavity interaction can be adjusted to the strong-coupling regime ($C \gg 1$) with the photon antibunching effect being retained, which can strongly enhance the photon emission rate and narrow the arrival-time distribution of single photons. Additionally, in our cavity emitter the single photons are nondeterministically produced at random times, since the system is continuously driven by an external laser field, for which it is better to apply laser pulses to trigger the single-photon emission.

For a single-photon emitter composed of interacting atoms driven by $\pi$-pulse sequence, the atomic system rarely emits two fluorescence photons simultaneously after a single excitation $\pi$ pulse. Both the pulse duration and the collective

spontaneous emission time affect the predetermined times of the system emitting single photons. Efficiently reducing the $\pi$-pulse width leads to a deterministic single-photon generation limited by the quantum system itself. However, in the meanwhile the two-photon emission weakens the nonclassical property of fluorescence because of the enhanced atom-field interaction. Moreover, efficiently collecting fluorescence photons is still a challenge in experiments.

Since the relevant techniques of manipulating both external and internal dynamics of Sr atoms have been fully developed [32–36], our single-photon emitter is experimentally feasible. In a future study, we will investigate a single-photon emitter based on an ensemble of three-level atoms in a $\Lambda$-type configuration composed of $(5s5p)^3P_{0,2}$ and $(5s5p)^3D_1$ states, where a single-mode optical resonator is applied to couple one atomic-transition leg while the other transition leg is driven by $\pi$-pulse sequence. This emitter has a potential to work as a single-photon source based on a number of interacting atoms.

## ACKNOWLEDGMENTS

D. Yu would like to thank Michael R. Hush for many useful discussions. This work is supported by the EU-FET5, Grant No. QuILMI 295293.

[1] B. Lounis and M. Orrit, Rep. Prog. Phys. **68**, 1129 (2005).
[2] C. Santori, D. Fattal, J. Vučković, G. S. Solomon, and Y. Yamamoto, Nature (London) **419**, 594 (2002).
[3] N. Gisin, G. Ribordy, W. Tittel, and H. Zbinden, Rev. Mod. Phys. **74**, 145 (2002).
[4] E. Knill, R. Laflamme, and G. J. Milburn, Nature (London) **409**, 46 (2001).
[5] H. J. Kimble, M. Dagenais, and L. Mandel, Phys. Rev. Lett. **39**, 691 (1977).
[6] F. Diedrich and H. Walther, Phys. Rev. Lett. **58**, 203 (1987).
[7] B. Lounis and W. E. Moerner, Nature (London) **407**, 491 (2000).
[8] P. Michler, A. Kiraz, C. Becher, W. V. Schoenfeld, P. M. Petroff, L. Zhang, E. Hu, and A. Imamoglu, Science **290**, 2282 (2000).
[9] H. J. Kimble, M. Dagenais, and L. Mandel, Phys. Rev. A **18**, 201 (1978).
[10] N. Schlosser, G. Reymond, and P. Grangier, Phys. Rev. Lett. **89**, 023005 (2002).
[11] P. B. R. Nisbet-Jones, J. Dilley, D. Ljunggren, and A. Kuhn, New J. Phys. **13**, 103036 (2011).
[12] E. Urban, T. A. Johnson, T. Henage, L. Isenhower, D. D. Yavuz, T. G. Walker, and M. Saffman, Nat. Phys. **5**, 110 (2009).
[13] J.-F. Huang, J.-Q. Liao, and C. P. Sun, Phys. Rev. A **87**, 023822 (2013).
[14] R. H. Lehmberg, Phys. Rev. A **2**, 883 (1970).
[15] Deshui Yu [Phys. Rev. A (to be published)].
[16] T. Bienaimé, R. Bachelard, N. Piovella, and R. Kaiser, Fortschr. Phys. **61**, 377 (2013).
[17] M. Keller, B. Lange, K. Hayasaka, W. Lange, and H. Walther, Nature (London) **431**, 1075 (2004).
[18] C. Brunel, B. Lounis, P. Tamarat, and M. Orrit, Phys. Rev. Lett. **83**, 2722 (1999).
[19] A. Kuhn, M. Hennrich, and G. Rempe, Phys. Rev. Lett. **89**, 067901 (2002).
[20] C. Bechera, A. Kiraz, P. Michler, W. V. Schoenfeld, P. M. Petroff, L. Zhang, E. Hu, and A. Imamoglu, Physica E **13**, 412 (2002).
[21] B. Olmos, D. Yu, Y. Singh, F. Schreck, K. Bongs, and I. Lesanovsky, Phys. Rev. Lett. **110**, 143602 (2013).
[22] C. Becker, P. Soltan-Panahi, J. Kronjäger, S. Dörscher, K. Bongs, and K. Sengstock, New J. Phys. **12**, 065025 (2010).
[23] The ring cavity is applied here so as to reduce the difference of atom-cavity coupling strengths for different atomic individuals because of the mismatch between wavelengths of the optical lattice and cavity mode.
[24] X. Zhou, X. Xu, X. Chen, and J. Chen, Phys. Rev. A **81**, 012115 (2010).
[25] K. Mølmer, Y. Castin, and J. Dalibard, J. Opt. Soc. Am. B **10**, 524 (1993).
[26] H. J. Kimble, Phys. Scr., T **76**, 127 (1998).
[27] H. G. Barros, A. Stute, T. E. Northup, C. Russo, P. O. Schmidt, and R. Blatt, New J. Phys. **11**, 103004 (2009).
[28] M. Hennrich, T. Legero, A. Kuhn, and G. Rempe, Phys. Rev. Lett. **85**, 4872 (2000).
[29] J. McKeever, A. Boca, A. D. Boozer, R. Miller, J. R. Buck, A. Kuzmich, and H. J. Kimble, Science **303**, 1992 (2004).
[30] C. Matthiesen, A. N. Vamivakas, and M. Atatüre, Phys. Rev. Lett. **108**, 093602 (2012).
[31] B. Darquié, M. P. A. Jones, J. Dingjan, J. Beugnon, S. Bergamini, Y. Sortais, G. Messin, A. Browaeys, and P. Grangier, Science **309**, 454 (2005).
[32] M. Takamoto, F.-L. Hong, R. Higashi, and H. Katori, Nature (London) **435**, 321 (2005).
[33] T. Akatsuka, M. Takamoto, and H. Katori, Nat. Phys. **4**, 954 (2008).
[34] T. Akatsuka, M. Takamoto, and H. Katori, Phys. Rev. A **81**, 023402 (2010).
[35] M. Takamoto, H. Katori, S. I. Marmo, V. D. Ovsiannikov, and V. G. Pal'chikov, Phys. Rev. Lett. **102**, 063002 (2009).
[36] S. Stellmer, M. K. Tey, B. Huang, R. Grimm, and F. Schreck, Phys. Rev. Lett. **103**, 200401 (2009).